AIAA 2003-0366

Broadband Noise Predictions for an Airfoil in a Turbulent Stream

J. Casper and F. Farassat
NASA Langley Research Center
Hampton, Virginia

P. F. Mish and W. J. Devenport
Virginia Polytechnic Institute and State University
Blacksburg, Virginia

41st Aerospace Sciences Meeting & Exhibit
January 6–9, 2002
Reno, Nevada

BROADBAND NOISE PREDICTIONS FOR AN AIRFOIL IN A TURBULENT STREAM

J. Casper* and F. Farassat†
NASA Langley Research Center
Hampton, Virginia

P. F. Mish‡ and W. J. Devenport§
Virginia Polytechnic Institute and State University
Blacksburg, Virginia

Abstract

Loading noise is predicted from unsteady surface pressure measurements on a NACA 0015 airfoil immersed in grid-generated turbulence. The time-dependent pressure is obtained from an array of synchronized transducers on the airfoil surface. Far field noise is predicted by using the time-dependent surface pressure as input to Formulation 1A of Farassat, a solution of the Ffowcs Williams – Hawkings equation. Acoustic predictions are performed with and without the effects of airfoil surface curvature. Scaling rules are developed to compare the present far field predictions with acoustic measurements that are available in the literature.

Nomenclature

b	=	airfoil semi-span (m)
C	=	airfoil chord (m)
c_0	=	ambient sound speed (m/s)
f	=	frequency (Hz)
g	=	velocity-to-pressure transfer function
k	=	ω/U, convective wave number (rad/m)
$\mathcal{L}$	=	streamwise integral length scale
M	=	Mach number
ΔP	=	unsteady surface pressure jump (Pa)
p	=	unsteady surface pressure (Pa)
p'	=	sound pressure radiated to observer (Pa)
$\vec{r}$	=	$\vec{x}-\vec{y}$, radiation vector (m)
t	=	observer time (s)
U	=	freestream speed (m/s)
u	=	streamwise turbulence component (m/s)
$\overline{u^2}$	=	streamwise mean-square turbulence (m^2/s^2)
$\vec{x}$	=	$[x_1, x_2, x_3]^T$, observer position (m)
$\vec{y}$	=	$[y_1, y_2, y_3]^T$, source position (m)
Φ_{33}	=	turbulence upwash PSD (m^4/ rad^2-s^2)
ϕ_n	=	random phase variable (rad)
λ	=	c_0 / f, acoustic wavelength (m)
θ	=	radiation angle from surface in Fig. 2 (m)
ρ_0	=	ambient density (kg/m^3)
τ	=	source time (s)
ω	=	circular frequency (rad/s)
ψ	=	directivity angle in Fig. 13 (rad)
$(\ )_{\text{ret}}$	=	evaluated at retarded time $t - r/c_0$

1. Introduction

The current work is focused on the correlation of unsteady surface pressure measurements to far field noise. The acoustic analogy [1] provides a framework for this correlation in the time domain. Noise due to unsteady surface loading is mathematically described by the loading source term, or "dipole term," of the Ffowcs Williams – Hawkings (FW-H) equation [2]. Because

* Research Scientist, Computational Modeling and Simulation Branch, AIAA Senior Member.
† Senior Research Scientist, Aeroacoustics Branch, AIAA Associate Fellow.
‡ Graduate Student, Aerospace and Ocean Engineering Dept., AIAA Student Member.
§ Professor, Aerospace and Ocean Engineering Dept., AIAA Senior Member.

the noise due to airflow over a rigid surface is typically dominated by dipole radiation, the acoustic formulations presented in this work are determined by solutions of the FW-H equation with the loading source term, i.e., the thickness and quadrupole terms are neglected.

The solution of the FW-H equation can be written in many forms. Acoustic predictions in the present work are performed with the loading noise version of Formulation 1A, of Farassat [3]. In its complete form, Formulation 1A is in current use throughout industry for the design of helicopter rotor blades. The version of Formulation 1A presented herein accounts for loading noise of an airfoil in motion and the effects of surface curvature.

In [4], far field predictions similar to those of the current study were reported and shown to compare favorably with experimental measurements of Paterson and Amiet [5]. Formulation 1B [4] was applied to the prediction of far field noise due to incident turbulence on a NACA 0012 airfoil at tunnel speeds ranging from 40 m/s to 165 m/s. Formulation 1B is a recently developed solution of the FW-H equation that was shown in [4] to be equivalent to Formulation 1A. As input to Formulation 1B, the time-dependent airfoil surface pressure was generated by stochastic modeling of the incident turbulence and the airfoil response was approximated with a result from thin airfoil theory [6]. Formulation 1B was then used to predict the far field acoustic pressure as a function in time at a microphone located 2.25 m directly above the geometric center of the upper airfoil surface. The time-dependent acoustic signal was then Fourier analyzed to determine the spectral density of the far field noise.

In Fig. 1, the predicted far field spectra for all five tunnel speeds are shown to be in good agreement with the experimental measurements of Paterson and Amiet [5], particularly in the range of 200 Hz to 1500 Hz, where the spectra are peaked. Note, however, that the prediction is most in error, by approximately 5 dB, at the lowest tunnel speed. This error is consistent with the low speed prediction in [5]. This error results from the fact that, as the tunnel speed decreases, the wavelength of the aerodynamic disturbance decreases and eventually become of the order of the airfoil thickness. In this case, the airfoil-turbulence interaction is influenced by the airfoil geometry, in particular by the shape of the leading edge. Therefore, as the free-stream speed decreases, the modeling of the surface pressure with the use of a thin-airfoil transfer function becomes increasingly invalid.

One of the goals of the current study is to determine the extent of the error made when thin-airfoil assumptions are incorporated into low-speed incident turbulence noise predictions. In [4], both the input surface pressure and the acoustic formulation were based on the approximation of the airfoil geometry as a flat plate. In the current study, the effects of surface curvature are considered in regard to both input and the acoustic formulation.

The particular version of Formulation 1A to be used in this work is described in the following section. The simplified version used herein easily allows the formulation to be used with or without the effects of airfoil surface curvature. Section 3 describes the low-speed wind tunnel experiment of interest and the surface pressure measurements that are used to correlate unsteady loading on a NACA 0015 model to the far field. In Section 4, the flat-plate acoustic formulation is used to predict far field noise using time-dependent pressure on the airfoil surface. This surface pressure is first modeled with thin-airfoil theory and the results are compared with predictions that result from experimentally measured surface pressure. In Section 5, scaling rules are developed that are used to compare the present predictions with acoustic data from [5]. The inclusion of the effects of surface curvature in the acoustic formulation is discussed in Section 6, followed by some concluding remarks.

2. Acoustic Formulation

Formulation 1A [3] was developed as a method to incorporate acoustic prediction in the design of helicopter rotor blades. Because the tip speeds of rotor blades can approach the speed of sound, Formulation 1A accounts for noise from both loading and thickness sources. However, for the low Mach number flows of interest in the present work, thickness noise can be neglected. A further simplification results from uniform rectilinear flow. The following introduction is required for the presentation of Formulation 1A as it applies to the current problem of interest.

Consider a surface moving along a velocity vector $\vec{V}$. Let $f(x_1, x_2, x_3, t)$ denote a geometric function that is so defined that $f = 0$ on the surface and $f > 0$ exterior to the surface. The velocity vector and the

surface geometry are related to the coordinate axes as pictured in Fig. 2.

Denote by $\vec{x} = [x_1, x_2, x_3]^T$ the position of an observer, and by $\vec{y} = [y_1, y_2, y_3]^T$ the position of a source point on the surface (Fig. 2). The unsteady pressure $p(\vec{y}, \tau)$ on the surface gives rise to sound that radiates along $\vec{r} = \vec{x} - \vec{y}$ to the observer. Note that the surface pressure is evaluated at source time τ. The sound is described by $p'(\vec{x}, t)$, the perturbation pressure that arrives at the point (x_1, x_2, x_3) at time *t*. For the case of uniform rectilinear motion, Formulation 1A can be expressed in the form

$$4\pi\, p'(\vec{x},t) = \frac{1}{c_0}\int_{f=0}\left[\frac{\partial p/\partial\tau\,\cos\theta}{r(1-M_r)^2}\right]_{\text{ret}} dS \; + \qquad (1)$$

$$\int_{f=0}\left[\frac{p(\cos\theta - M_n)}{r^2(1-M_r)^2}\right]_{\text{ret}} dS - \int_{f=0}\left[\frac{p\cos\theta\,(M_r - M^2)}{r^2(1-M_r)^3}\right]_{\text{ret}} dS$$

The subscript "ret" denotes evaluation at retarded time $t - r/c_0$, and θ is the angle subtended by the radiation vector and the surface normal $\hat{n}$ (Fig. 2.). The term $M_r = \vec{M}\cdot\hat{r}$ is the Mach number in the radiation direction, where $\vec{M} = \vec{V}/c_0$ is the local Mach number vector of the surface. Also, $M_n = \vec{M}\cdot\hat{n}$ is the Mach number in the direction of $\hat{n}$. Note that, in the case of a flat-plate geometry in the plane $x_3 = 0$, the surface normal $\hat{n}$ becomes $\hat{e}_3$, the vertical coordinate vector, and M_n vanishes.

3. Experimental Surface Pressure

3.1. Experiment Description & Instrumentation

Measurements of unsteady surface pressure were performed with an instrumented NACA 0015 airfoil. The model completely spans the 1.83 m test section of the Virginia Tech Stability Wind Tunnel and has a 0.6096 m chord. This facility test section is 7.32 m long with a 1.83 m-square cross section. At 30 m/s, flow through the empty test section is virtually uniform and of low turbulence intensity (<0.05%). Background noise levels are acceptable for the aerodynamic measurements of interest [7, 8].

Measurements for the present study were made at a tunnel speed of 30 m/s (Re = 1.17 x 10^6) with the model at zero angle of attack (Results at non-zero angles of attack are reported in [9, 10, 11]). A square bi-planar grid is mounted 5.82 m upstream of the airfoil leading edge in the wind tunnel contraction. At the grid location the cross-sectional area is 32% larger than that of the test section. The grid has a mesh size of 30.5 cm, an open area ratio of 69.4%, and generates turbulence with a streamwise integral length scale $\mathcal{L}$ = 8.18 cm (13% chord) at 30 m/s. The resulting streamwise turbulence intensity at 30 m/s is 3.93%.

The airfoil is instrumented with an array of 96 Sennheiser KE 4-211-2 microphones, embedded in the upper and lower airfoil surfaces over the center 58.5 cm of its span. Fig. 3 shows the array layout on the upper surface of the foil. The layout on the lower surface is a mirror image. Microphones are located in chordwise rows between 1% and 85% of the chord length from the leading edge, and at spanwise separations of between 1% and 96% chord. The spanwise distribution of microphones is designed to take advantage of the homogeneity of the flow in this direction so that the 8 spanwise stations together define some 25 approximately logarithmically spaced spanwise separations. The Sennheiser microphones are calibrated from 4 Hz to 20 kHz with an uncertainty of ±1.5 dB.

The effects of the ambient acoustic field were assessed with pressure measurements made with no grid present. These measurements fall several decades in spectral level below measurements with the grid installed. Therefore, pressure data that is taken with the grid installed is considered to be uncontaminated by ambient acoustic field pressure fluctuations. Further details on instrumentation and apparatus can be found in [9, 10, 11].

3.2. Instantaneous Pressure Fluctuations

The dominant types of pressure fluctuations arising from the turbulence-airfoil interaction can be clearly revealed through contour plots of the instantaneous pressure. By considering a contour plot of time series in space and time, the propagation speed of various types of pressure fluctuations occurring on the surface of the airfoil are shown. If the spatial axis is normalized on chord length *C* and the time is normalized as *tU*/*C*, a fluctuation which is convecting with the mean free stream velocity will have a 1 to 1 slope on such a contour plot. Similarly, a fluctuation propagating downstream at sound speed will have a slope of $(U + c_0)/U$, approximately 12 to 1, and a fluctuation

propagating upstream at sound speed will have a slope of $(U - c_0)/U$, approximately 10 to 1.

Fig. 4 presents such a sample contour plot of the instantaneous surface pressure field on both the pressure and suction sides of the airfoil (positive *x*-axis indicates pressure side of airfoil). The time series have been adjusted to account for the dynamic response of each microphone and are high pass filtered at 10 Hz to remove low frequency uncertainties that arise from the microphone calibration. Low pass filtering is performed by the data acquisition system (HP1432) to preclude aliasing of the data beyond 500Hz. Fig. 4 shows evidence of eddies striking the leading edge and causing an instantaneous adjustment of angle of attack and consequently, lift (due to the upwash velocity) which is propagated at sound speed (slope of 12:1) across the chord. Additionally, a pressure rise in the leading edge region on one side of the airfoil develops which is balanced by a pressure reduction on the opposing side. After the sound speed adjustment in lift, the eddy begins to convect down the chord close to the mean free stream velocity (1:1 slope). Note that the space-time correlations show that surface pressure fluctuations on the forward part of the airfoil are dominated by disturbances that propagate along the 12:1 slope [10, 11].

4. Acoustic Predictions

4.1. Problem Description

Far field noise is now predicted for the experiment described in Section 3. In order to perform the calculations, a coordinate system is established as in Fig. 5, with the airfoil's mean-chord plane of symmetry defined by $\{0 \le x_1 \le C\} \times \{-b \le x_2 \le b\}$ in the plane $x_3 = 0$. The airfoil surface profile is determined by the function $x_3 = F(x_1)$, which is well known for NACA series airfoil profiles, e.g., [12]. For the acoustic predictions in this section, the airfoil geometry will be modeled as a flat plate in the plane $x_3 = 0$. Therefore, a source location on the surface is of the form $\vec{y} = [y_1, y_2, 0]^T$, and the surface normal is $\hat{n} = [0,0,1] = \hat{e}_3$ at every point. The effects of surface curvature will be discussed in Section 6.

An observer is placed at a distance r = 2.25 m directly above the geometric center of the mean-chord plane, i.e. $\vec{x} = [C/2, 0, r]^T$, as in Fig. 5. This observer location is chosen to be the same as the primary microphone location in [5]. In Section 5, scaling rules are developed to scale the measurements in [5] to serve as estimates against which the present predictions can be compared.

Noise is predicted, using Eq. (1) with surface pressure given by a theoretical formulation and by experimental measurements as described in Section 3. Results from both cases are compared.

4.2. Analytic Surface Pressure

In [13], Amiet developed a frequency-domain formulation for the prediction of noise due to an airfoil immersed in homogeneous, isotropic turbulence. The source in Amiet's formulation, i.e., the airfoil response to an unsteady surface pressure, was entirely characterized by the incident velocity field. The velocity field is thereby expressed as a linear superposition of periodic gusts that convect at the freestream speed *U* over a flat plate of finite chord and infinite span.

In [4], a time-domain surface pressure model was developed along the same lines as the frequency-domain source model of Amiet [13]. As in Amiet's analysis, it was determined that, for an observer in the plane $x_2 = 0$, only the zero spanwise wave number in the turbulent velocity spectrum contributes to the acoustic signal. This result greatly simplifies the source model and enables the surface pressure $p(\vec{y}, \tau)$ in Eq. (1) to be expressed as a function of time *t*, the streamwise surface coordinate y_1, and the streamwise wave number $k_1 = \omega / U$. (See [4] for details.) Thus, for acoustic prediction purposes, the unsteady pressure jump ΔP across the airfoil can be approximated by

$$\Delta P(y_1, t) \approx 2\pi\rho_0 U \sum_{n=-N}^{N} A_n \, e^{i\phi_n} \, g(y_1, k_{1,n}) \, e^{i k_{1,n} U t} \qquad (2)$$

$$k_{1,n} = n\Delta k_1, \qquad n = 0, \pm 1, \pm 2, \ldots, \pm N$$

$$\Delta k_1 = k_{1,N} / N$$

where ρ_0 is the ambient density and $g(y_1, k_1)$ is a transfer function that is derived from thin airfoil theory [6]. Also, $k_{1,N}$ is an "upper cutoff" wave number, beyond which the spectral amplitude is considered negligible or is out of range of experimental measurement. The phase angles $\{\phi_n\}$ are independent random variables uniformly distributed on $[0, 2\pi]$. The gust amplitudes $\{A_n\}$ are given by

$$A_n = [\Phi_{33}(k_{1,n},0)\Delta k_1]^{\frac{1}{2}} \qquad (3)$$

where $\Phi_{33}(k_1,k_2)$ is the two-component power spectral density (PSD) of the upwash component of the turbulence. An expression for this upwash PSD is obtained in [13] by integrating the von Karman formula [14] over all k_3; the result is:

$$\Phi_{33}(k_1,k_2) = \frac{4}{9\pi}\frac{\overline{u^2}}{k_e^4}\frac{k_1^2 + k_2^2}{[1+(k_1/k_e)^2+(k_2/k_e)^2]^{7/3}} \qquad (4a)$$

where $\overline{u^2}$ is the streamwise mean-square turbulence, and k_e is the peak wave number given by

$$k_e = \frac{\sqrt{\pi}}{\mathcal{L}}\frac{\Gamma(5/6)}{\Gamma(1/3)} \approx \frac{0.747}{\mathcal{L}} \qquad (4b)$$

where $\mathcal{L}$ is the streamwise integral length scale. Evaluation of the time-dependent surface pressure by Eqs. (2) and (3) is consistent with stochastic modeling theory, e.g., [15]. Eq. (1) will be applied in a real-valued, one-sided form ($0 \le n \le N$); details can be found in [4].

In order to use the above analytical formulation as input to an acoustic prediction, values for the integral length scale and the mean-square turbulence are taken from the experimental measurements described in Section 3.1. The lower bound on frequency, and therefore the fundamental frequency, is chosen to be 10 Hz; the upper bound is chosen at 2500 Hz, with a numerical bandwidth $\Delta f = 10$ Hz. The physical duration of the calculation is one period of the fundamental, i.e., $T = 0.1$ s. The time-step is chosen as $\Delta t = T/2N$ so that the numerical solution is sampled at the Nyquist frequency. The surface integration in Eq. (1) is performed on a 100×10 surface grid shown in Fig. 6. The reason for the coarseness of the mesh in the y_2 direction is that the analytic surface pressure has no variation in that direction, and for the span length and observer distance of interest, the prediction is relatively insensitive to additional resolution in y_1 [4]. Note that the grid is clustered near the leading edge because of the rapid increase in the transfer function $g(y_1,k_1)$ near $x = 0$ (see [4]).

4.3. Experimental Surface Pressure

The prediction of incident turbulence noise with measured surface pressure will follow the same reasoning as with the analytical formulation in Section 4.2. That is, the spanwise variation of the surface pressure will be ignored with respect to its influence on the acoustic signal.

The pressure jump across the mean chord plane will be modeled with measurements from the chordwise array of 13 transducers that are located between 1% and 85% of the chord length (Fig. 3). For integration purposes, the pressure jump will be considered piecewise constant along the chord. To this end, let the set $\{y_{1,i}\}_{i=1}^{14}$ denote a discretization of the chord with

$$0 = y_{1,1} < \cdots < y_{1,i} < y_{1,i+1} < \cdots < y_{1,14} = C \qquad (5)$$

such that each interval $(y_{1,i}, y_{1,i+1})$ in Eq. (5) contains a transducer location $y_{1,m}$ at or near its center. Then, for acoustic prediction purposes, the surface distribution of the pressure jump is

$$\Delta P(y_1,t) = \Delta P(y_{1,m},t), \quad y_{1,i} < y_1 \le y_{1,i+1} \qquad (6a)$$

on each of the 13 intervals determined by the discretization in Eq. (5). The pressure jump at each transducer location is calculated by the difference between simultaneously measured pressures on the lower and upper surfaces, i.e.,

$$\Delta P(y_{1,m},t) = p_{\text{lower}}(y_{1,m},t) - p_{\text{upper}}(y_{1,m},t) \qquad (6b)$$

The grid in Fig. 7 shows the 13×10 surface elements that are used to integrate the surface pressure in Eq. (6a). For purposes of the Fourier analysis that is required to calculate the far field spectrum, the measured surface pressure is assumed to be of spectral content that is dictated by its time duration T = 1.28 s and a sampling rate of 1600 Hz. On this basis, the measured data is presumed periodic with a frequency range up to 800 Hz. However, the low pass filtering of the data (Section 3.2) curtails reliability of the data beyond 500 Hz. Furthermore, an extensive analysis of these data indicates that measurements from transducers located downstream of the 20%-chord location contain enough turbulent boundary layer noise to make the contribution from the freestream turbulence difficult, if not impossible to detect. Therefore, the pressure jump in Eq. (6a) is zeroed for all stations downstream of the 20%-chord location, i.e., for $m \ge 8$.

4.4 Acoustic Results

Because the spanwise variation in the surface pressure is neglected, the amount of physical span that is chosen for the acoustic prediction is arbitrary and is chosen as $2b$ = 0.53 m, as in the experiment in [5].

Fig. 8 shows the far field spectra for the two input surface pressure jumps, analytical and experimental. The spectrum with experimental input has been averaged over 128 records. It is not surprising that the theoretical prediction is higher than the prediction with experimental input. This result is consistent with the over-prediction of the theory relative to acoustic measurements at the lowest tunnel speed in Fig. 1.

Some words on the accuracy of the prediction with measured surface pressure are in order. Unfortunately, far field measurements for the present experiment are not available for comparison. Far field measurements from [5] will be scaled for this purpose in Section 5. There is also the issue of using the data in the form of a pressure jump across a flat plate. This should be a reasonable approximation, providing that the observer is sufficiently far away from the plane of the airfoil mean chord, where the effects of surface curvature cannot be ignored, as will be discussed in Section 6.

5. Scaling Rules

5.1. Amplitude Scaling

For scaling purposes, it is convenient to consider the relative contributions of the terms in Eq. (1), under the conditions of low Mach number and an observer that is in the acoustic and geometric far fields, i.e.

$$M \ll 1, \qquad r \gg \lambda, \qquad r \gg C \tag{7}$$

where $\lambda = c_0 / f$ is a typical acoustic wavelength of interest. In this case, θ and M_r are small, and the differences in retarded time can be neglected. If, in addition, the surface is in the plane $x_3 = 0$, then M_n vanishes. Under these conditions, the first integral in Eq. (1) clearly dominates the acoustic signal, as it is proportional to $1/r$, whereas the second and third integrals are proportional to $1/r^2$. Therefore, the acoustic formulation is approximated by

$$4\pi\, p'(\vec{x},t) \approx \frac{1}{c_0 \bar{r}} \int_{f=0} \frac{\partial}{\partial \tau}\, p(\vec{y},\bar{\tau})\, dS \tag{8}$$

where $\bar{r}$ is a mean value of the distance r, and $\bar{\tau} = t - \bar{r} / c_0$ is the mean retarded time.

If the surface pressure jump in Eq. (2) is substituted for $p(\vec{y},\bar{\tau})$ in Eq. (8), and the surface $\tilde{f} = 0$ is defined by the planar geometry in Section 4.1, the result is

$$p'(\vec{x},t) \approx \frac{b\rho_0 U^2}{c_0 \bar{r}} \sum_{n=-N}^{N} A_n\, I_n\, i k_{1,n}\, e^{i(k_{1,n} U \bar{\tau} + \phi_n)} \tag{9a}$$

where

$$I_n = \int_0^C g(y_1, k_{1,n})\, dy_1 \tag{9b}$$

Now, consider the comparison of noise levels between two experimental states A and B. What distinguishes these "states" is the variability in the airfoil model and the flow field. For the present problem, these variables are b, C, U, $\overline{u^2}$, and $\mathcal{L}$. The measure of comparison is the sound pressure level (SPL), defined by

$$SPL(f_n) = 10 \log \left\{ \frac{\overline{P_n^2}}{P_{\text{ref}}^2} \right\} \tag{10}$$

where $\overline{P_n^2}$ is the PSD of the acoustic pressure-squared at the frequency f_n, the over-bar denotes a time average, and P_{ref} is a reference pressure most commonly taken to be 20 μPa. The values of the pressure spectrum $\{P_n\}$ are the resulting amplitudes of a Fourier analysis of the time series in Eq. (9a). Suppressing the spatial dependence, Eq. (9a) can be re-written in the form

$$p'(t) = \sum_{n=-N}^{N} \hat{q}_n\, e^{i\omega_n \bar{\tau}} \tag{11a}$$

where

$$\hat{q}_n = \frac{b\rho_0 U^2}{c_0 \bar{r}} A_n\, I_n\, i k_{1,n}\, e^{i\phi_n} \tag{11b}$$

It can be shown (see e.g., [16]) that the time average of $[p'(t)]^2$ can be evaluated as

$$\overline{[p'(t)]^2} = \overline{[p'(t)][p'(t)]^*} = \sum_{n=-N}^{N} \left| \hat{q}_n \right|^2 = \sum_{n=0}^{N} \overline{P_n^2} \tag{12}$$

where the star superscript denotes a complex conjugate.

In order to compare noise levels between the two states, let the subscript notation $(\cdot)_A$ and $(\cdot)_B$

represent quantities that are evaluated with respect to states *A* and *B*, respectively. Using Eqs. (10) – (12), the desired *SPL* differential, for $0 \le n \le N$, is evaluated by

$$\begin{aligned}\left[SPL(f_n)\right]_B - \left[SPL(f_n)\right]_A &= 10\log\left\{\frac{(\overline{P_n^2})_B}{(\overline{P_n^2})_A}\right\} \\ &= 10\log\left\{\frac{|\hat{q}_n|_B^2}{|\hat{q}_n|_A^2}\right\}\end{aligned} \tag{13}$$

where

$$|\hat{q}_n|^2 = \hat{q}_n\,\hat{q}_n^* = \frac{b^2\rho_0^2 U^4}{c_o^2\,\bar{r}^2}\,k_n^2\,|I_n|^2 A_n^2 \tag{14}$$

Note that the surface pressure amplitudes $\{A_n\}$ are presumed real. Using the result of Eq. (14), the *SPL* differential in Eq. (13) becomes

$$\left[SPL(f_n)\right]_B - \left[SPL(f_n)\right]_A = \tag{15}$$

$$10\log\left\{\left[\frac{\bar{r}_A}{\bar{r}_B}\right]^2\left[\frac{b_B}{b_A}\right]^2\left[\frac{U_B}{U_A}\right]^4\left[\frac{(k_n)_B}{(k_n)_A}\right]^2\left[\frac{|I_n|_B}{|I_n|_A}\right]^2\left[\frac{(A_n)_B}{(A_n)_A}\right]^2\right\}$$

In [6], it is shown that I_n is proportional to $1/k_n$. Using this result and the definition of A_n in Eq. (3), the scaling rule in Eq. (15) becomes

$$\left[SPL(f_n)\right]_B - \left[SPL(f_n)\right]_A = \tag{16}$$

$$10\log\left\{\left[\frac{\bar{r}_A}{\bar{r}_B}\right]^2\left[\frac{b_B}{b_A}\right]^2\left[\frac{U_B}{U_A}\right]^4\left[\frac{(\Phi_{33})_B}{(\Phi_{33})_A}\right]\left[\frac{\Delta k_B}{\Delta k_A}\right]\right\}$$

where Φ_{33} is interpreted as $\Phi_{33}(k_1,0)$, the zero-th spanwise wave-number component of the upwash PSD defined in Eqs. (4a) and (4b).

5.2. Frequency Scaling

The effect of $|I_n|^2$ on the magnitude scaling in Eq. (15) has already been discussed. Its effect can be at least as significant in regard to the frequency f_n. The transfer function $g(y_1,k_{1,n})$ in Eq. (9b) contains the factor e^{ikC}, which makes for a linear proportionality between the frequency f_n and the chord length C [6]. Therefore, when $C_A \neq C_B$, $[SPL(f_n)]_A$ is not scaled to $[SPL(f_n)]_B$ at the same frequency f_n, as implied by Eq. (16). The proportionality between the two frequencies f_A and f_B is

$$f_B = \frac{C_A}{C_B}\,f_A \tag{17}$$

Note that the scaling rules in Eqs. (16) and (17) do not account for directivity. This is not a concern for the present problem where the observer location has been chosen to match the far field microphone position of Paterson and Amiet [5], whose far field data will be scaled for comparison.

5.3. Scaling for Predictions and Measurements

In order to test the validity of Eqs. (16) and (17), states *A* and *B* are as defined in Table I below.

State	C	U	$\overline{u^2}$	$\mathcal{L}$
A	23.00 cm	40 m/s	3.01 m^2/s^2	3.20 cm
B	60.96 cm	30 m/s	1.39 m^2/s^2	8.18 cm

Table I. Experimental States A and B.

These two states *A* and *B* are, respectively, the 40 m/s test case from Paterson and Amiet [5] in Fig. 1, and the present test case of Mish [9, 10]. Note that the observer distance of 2.25 m and the airfoil span of 0.53 m are the same for both states.

Fig. 9 shows theoretical acoustic predictions for states *A* and *B* in Table I, using the analytic surface pressure in Eqs. (2) – (4) as input to Eq. (1). The symbols represent a scaling prediction for state *B* that results from using the theoretical prediction for state *A* as input to Eqs. (16) and (17). The scaled results show excellent agreement with the State B prediction for frequencies above 100 Hz. The error is one dB or less for frequencies down to 40 Hz. The error is expected to increase for low frequencies because of the condition that relates the observer distance to the acoustic wavelength, given in Eq. (7). For a given problem, the lower frequency bound for acceptable scaling error is a function of the quantities in Eq. (7).

It is not surprising that the scaling results in Fig. 9 are so successful, because the scaling rules in Eqs. (16) and (17) are derived from the same theory that is used to predict the spectra in Fig. 9. The more important determination is the extent to which the far field

measurements in [5] will scale by these rules. Fig. 10 shows the acoustic data in Fig. 1, having applied the scaling rule in Eq. (16) with the 40 m/s case as the reference state A. Eq. (17) is not needed for the results in Fig. 10. The only scaling parameters for these data are U and $\overline{u^2}$, because the values of b, C, and $\mathcal{L}$ are constant for all five datasets. Note that the solid symbols in Fig. 1 have not been included in Fig. 10 because their values are suspect due to the low signal-to-noise ratio associated with those measurements [5].

Fig. 11 shows acoustic predictions for state *B* in Table I, using theoretical and experimentally measured surface pressure, as in Fig. 8. The symbols in this figure are scaled measurements, using the 40 m/s data from Paterson and Amiet [5] in Fig. 1 as the reference state. Although it is not disturbing that the scaled data lie between the two predictions, the maximum 7 dB difference between the scaled data and the prediction with measured surface pressure is an issue that remains to be resolved.

6. Surface Curvature Effects

The effects of the airfoil surface curvature are now considered. As previously noted, surface curvature is not expected to have a significant influence on the far field spectra for an observer located sufficiently far away from the plane of the mean chord. Fig. 12 shows an acoustic prediction that includes the airfoil surface curvature terms in Eq. (1). Included in this plot is the prediction from Fig. 8 in which the airfoil is modeled as a flat plate. The difference is no more than approximately 2 dB throughout the spectrum.

It should be noted here that the use of a pressure jump with a curved surface is technically incorrect, as can be shown by a geometrical argument. In order to appropriately account for acoustic emissions from a curved airfoil surface, the local pressure $p(\vec{y},\tau)$ itself must be integrated over all points $\vec{y}$ on the upper and lower surfaces. The appropriate approach to the surface curvature problem is a topic for further research.

In order to qualitatively inspect the significance of surface curvature, the radiated noise is calculated at many locations on a circular path in the plane $x_2 = 0$, as shown in Fig. 13. The observer's trajectory (r, ψ) is determined by r = 2.25 m and $0 \le \psi \le 2\pi$. The *SPL* directivity for six frequencies is plotted in Figs. 14 and 15. The noise levels in both figures were determined with measured surface pressure input to Eq. (1), averaged over 128 records. In Fig. 14, it is clearly seen that the noise level goes to zero in the plane of the airfoil mean chord when the airfoil surface is modeled as a flat plate. However, when the surface normal accounts for the NACA 0015 profile, there are clearly nontrivial noise levels in the mean chord plane, as shown in Fig. 15. The curved surface has created an additional horizontal dipole. As discussed earlier in this section, these predictions do not accurately account for the surface curvature in the mean chord plane.

Concluding Remarks

Acoustic predictions have been performed in the time domain by a solution of the Ffowcs Williams – Hawkings equation and the use of experimentally measured surface pressure as input. Within the acoustic calculations, a NACA 0015 airfoil was modeled as a flat plate and including surface curvature. Acoustic predictions were also performed with a theoretical formula for surface pressure for comparison purposes. Scaling rules were developed to obtain an additional acoustic dataset for comparison. Issues that remain include a reassessment of scaling and an appropriate accounting for surface curvature with pointwise surface pressure as input.

Acknowledgment

The authors would like to thank Casey Burley and Tom Brooks of NASA Langley Research Center in Hampton, Virginia for their support under grant NAG-1-2272.

References

1. Lighthill, M. J., "On Sound Generated Aerodynamically. I. General Theory," *Proceedings of the Royal Society of London*, A 211, 1952, pp. 564 – 587.

2. Ffowcs Williams, J. E. and Hawkings, D. L., "Sound Generation by Turbulence and Surfaces in Arbitrary Motion," *Philosophical Transactions of the Royal Society*, A 264, 1969, pp. 321 – 342.

3. Farassat, F. and Succi, G. P., "The Prediction of Helicopter Rotor Discrete Frequency Noise," *Vertica*, Vol. 7, No. 4, 1983, pp. 309 – 320.

4. Casper, J. and Farassat, F., "A New Time Domain Formulation for Broadband Noise Predictions,"

International Journal of Aeroacoustics, Vol. 1, No. 3, pp. 207 – 240.

5. Paterson, R. W. and Amiet, R. K., "Noise and Surface Pressure Response of an Airfoil to Incident Turbulence," *AIAA Journal of Aircraft*, Vol. 14, No. 8, 1977, pp. 729 – 736.
6. Amiet R K, 1976, "High-frequency thin airfoil theory for subsonic flow", *AIAA Journal*, vol. 14, no. 8, pp. 1076-1082.
7. Choi K and Simpson R L, 1987, "Some mean velocity, turbulence and unsteadiness characteristics of the Virginia Tech Stability Wind Tunnel", Report VPI-AOE-161, Virginia Tech, Blacksburg VA.
8. Larssen J V and Devenport W J, 1999, "Acoustic Properties of the Virginia Tech Stability Wind Tunnel", Rept. VPI-AOE-263, AOE Dept., Virginia Tech.
9. Mish, P. F., "Mean Loading and Turbulence Scale Effects on the Surface Pressure Fluctuations Occurring on a NACA 0015 Airfoil Immersed in Grid Generated Turbulence", Masters Thesis, Virginia Tech, June 2001.
10. Mish, P. F., "An Experimental Investigation of Unsteady Surface Pressure on Single and Multiple Airfoils in Turbulence", Ph.D. dissertation, Virginia Tech, to be published.
11. Mish, P. F., Devenport, W. J., and Borgoltz, A. G., "Evaluation and further analysis of unsteady pressure response measurements on an airfoil at angle of attack", 8th AIAA/CEAS Aeroacoustics Conference, Breckenridge, Colorado, 17-19 June 2002.
12. Abbott, I. H. and Von Doenhoff, A. E., *Theory of Wing Sections*, Dover Publications, New York, 1959.
13. Amiet R K, 1975, "Acoustic radiation from an airfoil in a turbulent stream", *Journal of Sound and Vibration*, vol. 41, no. 4, pp. 407 – 420.
14. Shinozuka, M. and Deodatis, G., "Simulation of Stochastic Processes by Spectral Representation," *Applied Mechanics Review*, Vol. 44, No. 4, 1991, pp. 191 – 204.
15. von Karman, T., "Progress in the Statistical Theory of Turbulence," *Journal of Marine Research*, Vol. 7, No. 3, 1948, pp. 252 – 264.
16. Pierce, A. D., *Acoustics*, Acoustical Society of America, New York, 1991.

Figures

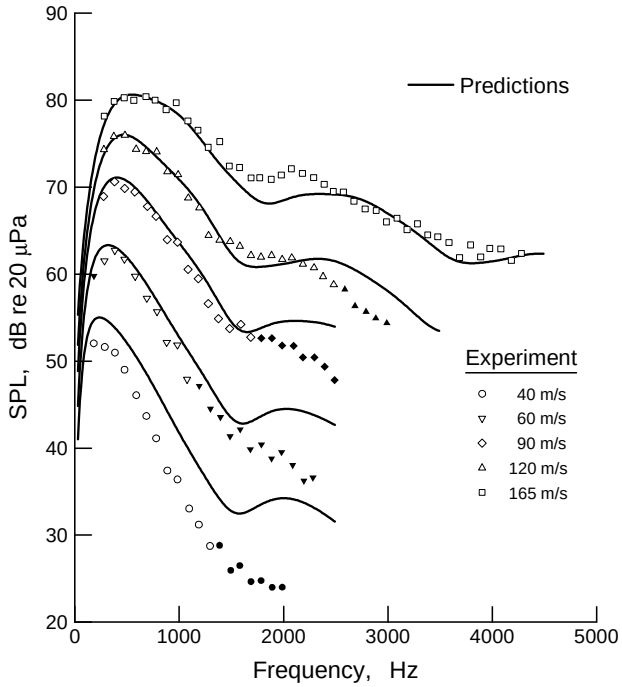

Figure 1. Incident turbulence noise spectra: predictions from [4], measurements from [5].

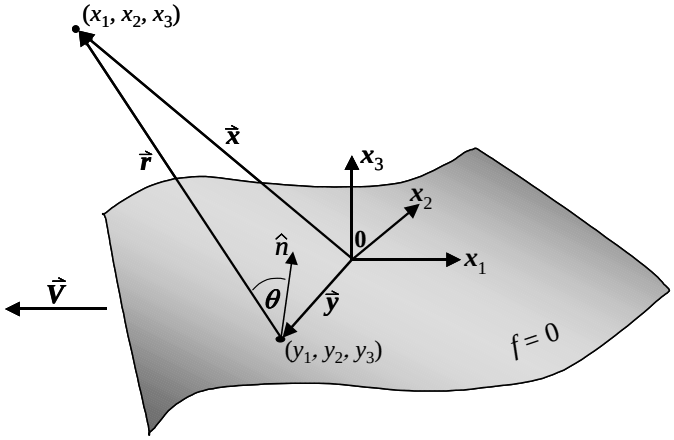

Figure 2. Schematic for Formulation 1A, Eq. (1).

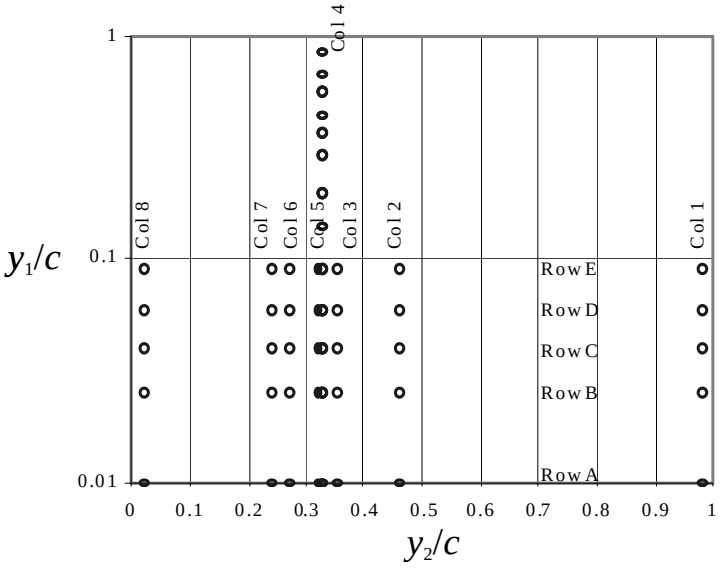

Figure 3. NACA 0015 microphone distribution.

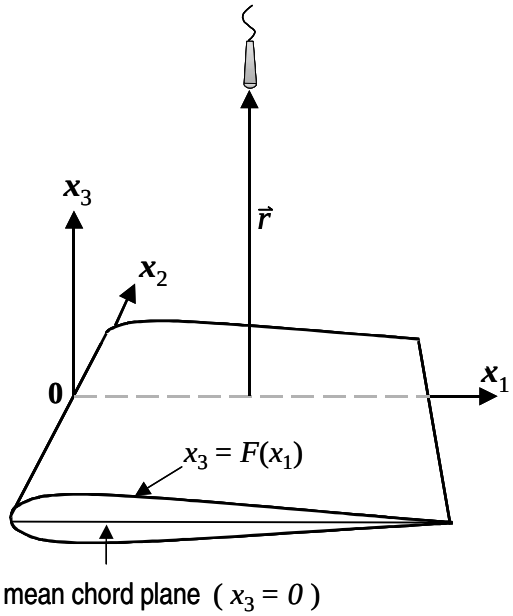

Figure 5. Schematic for acoustic calculation.

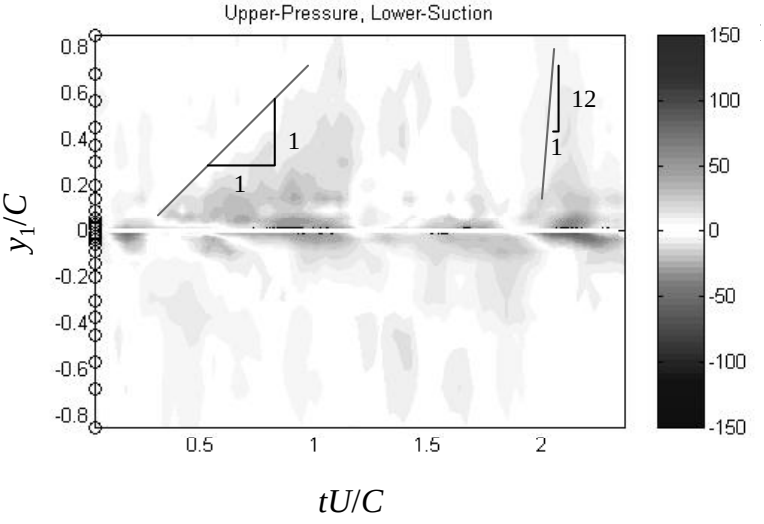

Figure 4. Instantaneous pressure (Pa) on the pressure and suction side of the airfoil (positive *x* values indicate pressure side)—data from Mish [9].

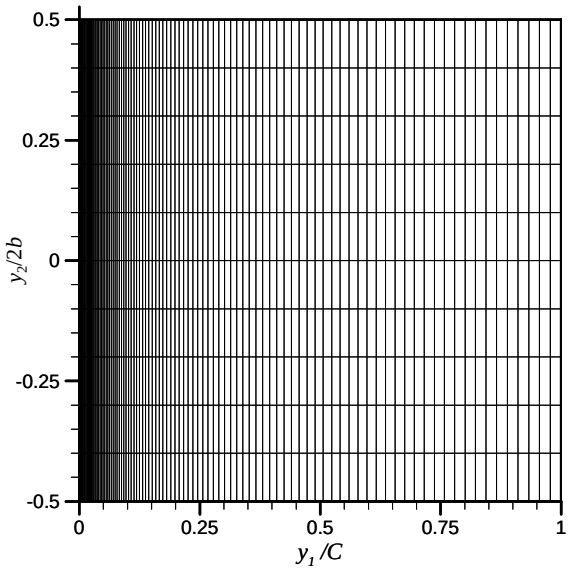

Figure 6. Surface mesh for acoustic prediction with analytic pressure input, Eqs. (2) – (4).

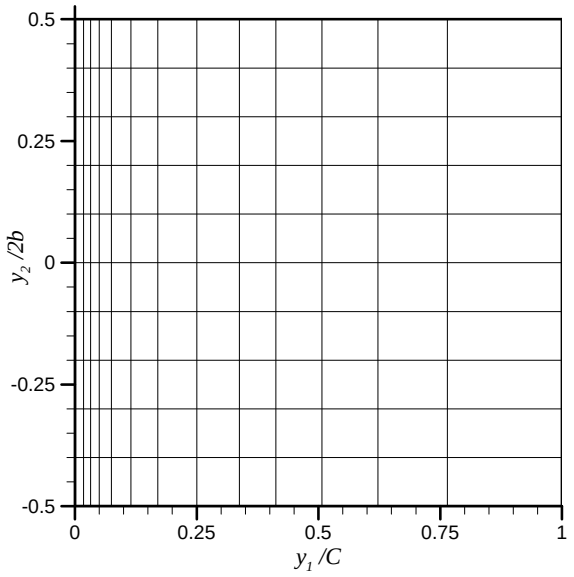

Figure 7. Surface mesh for acoustic prediction with experimental pressure input.

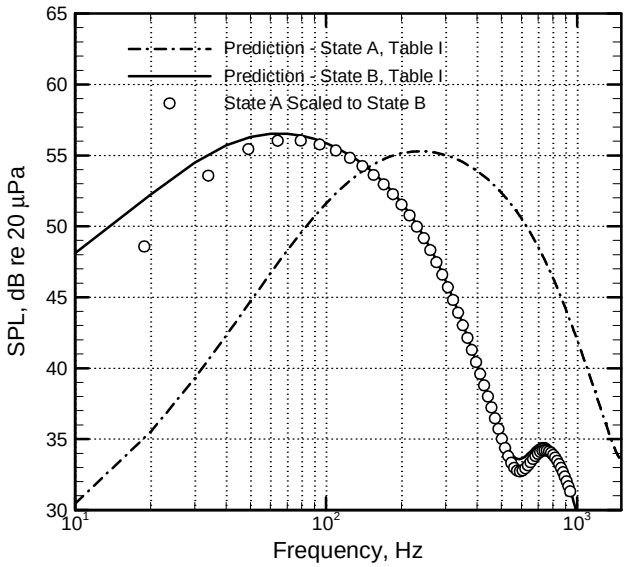

Fig. 9. Predictions for States A and B in Table I. Symbols represent the use of Eqs. (16) and (17) to scale State A to State B.

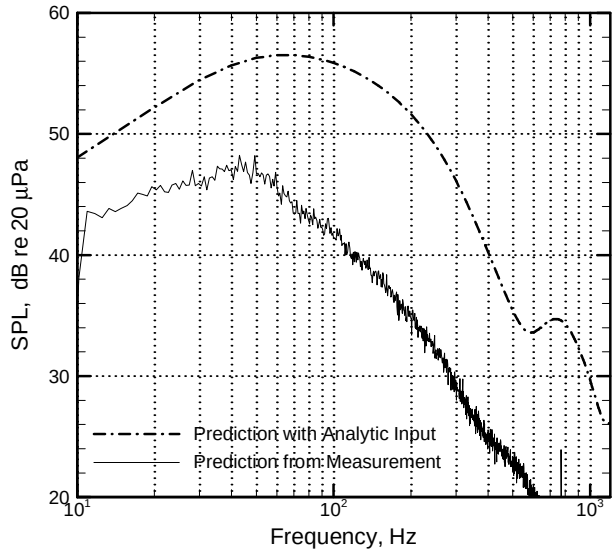

Figure 8. Far field spectra, r = 2.25 m, directly above airfoil, with flat-plate acoustic formulation

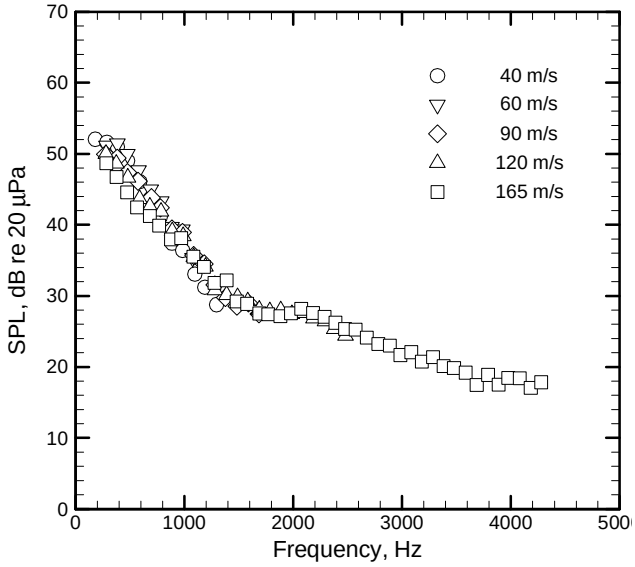

Fig. 10. Paterson and Amiet's [5] measurements, from Fig. 1, with scaling applied by Eq. (16) and U = 40 m/s as the reference state.

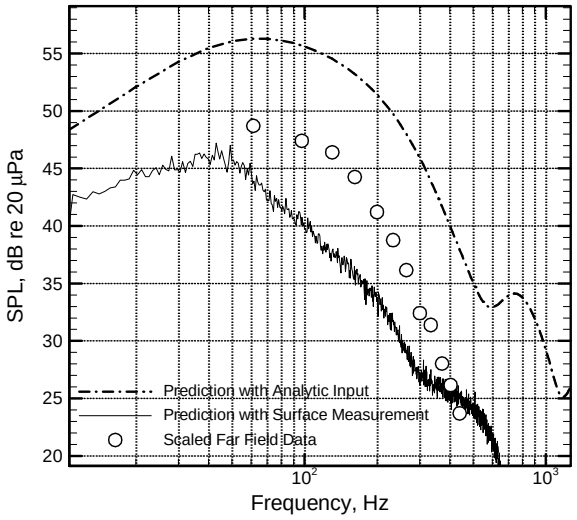

Fig. 11. Far field spectra with analytic input, measure input, and scaled acoustic measurement from [5].

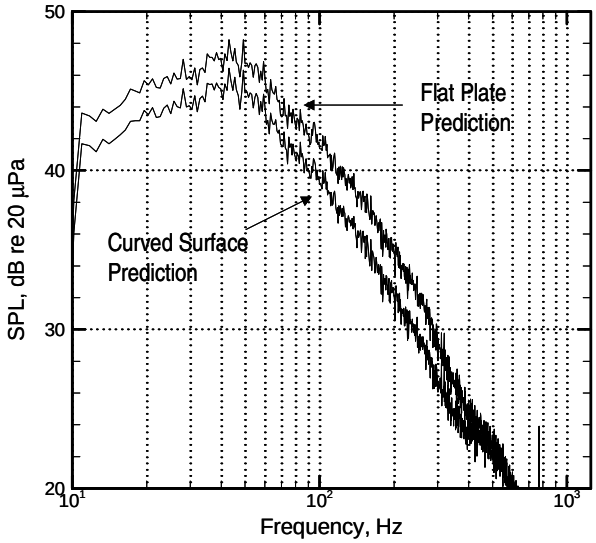

Fig. 12. Far field spectra predicted with measured surface pressure. Airfoil geometry modeled as flat plate and NACA 0015 profile.

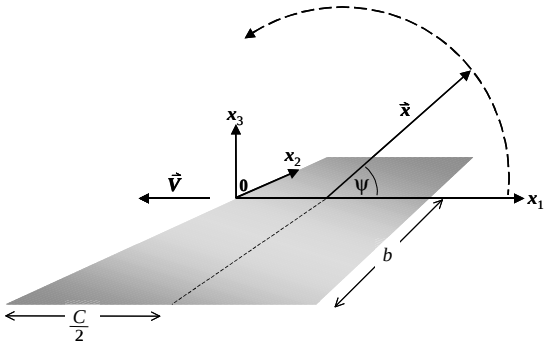

Fig. 13. Schematic for directivity calculation; observer in the plane $x_2 = 0$.

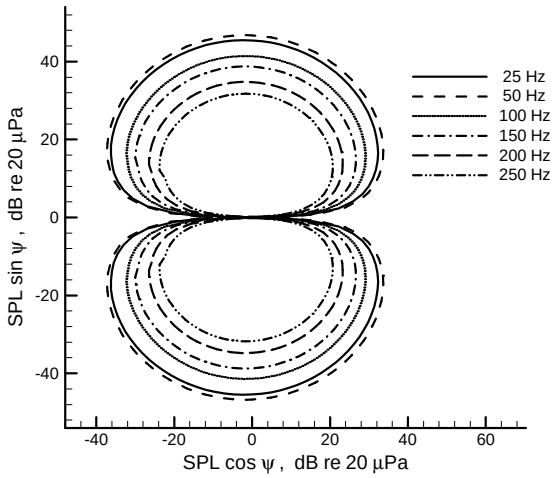

Fig. 14. Directivity; airfoil geometry modeled as flat plate.

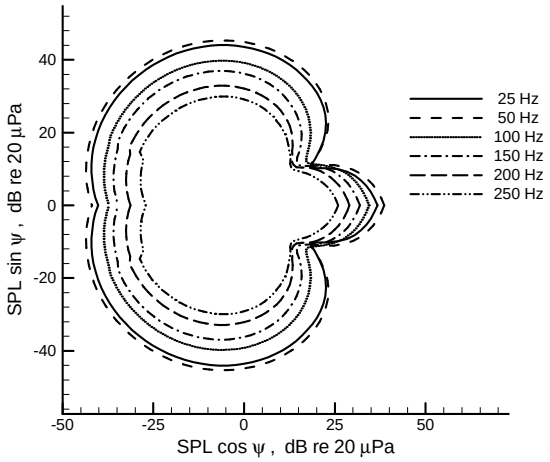

Fig. 15. Directivity; airfoil geometry modeled with NACA 0015 profile.